# Multiorbital spin-triplet pairing and spin resonance in the heavy-fermion superconductor $UTe_2$

Lei Chen[⊕],[1] Haoyu Hu[⊕],[1] Christopher Lane,[2] Emilian M. Nica,[3] Jian-Xin Zhu,[2] and Qimiao Si[1]

[1]*Department of Physics and Astronomy, Rice Center for Quantum Materials, Rice University, Houston, Texas, 77005, USA*
[2]*Theoretical Division and Center for Integrated Nanotechnologies, Los Alamos National Laboratory, Los Alamos, New Mexico 87545, USA*
[3]*Department of Physics, Arizona State University, Box 871504, Tempe 85287-1504, AZ, USA*

The heavy-fermion system $UTe_2$ is a candidate for spin-triplet superconductivity, which is of considerable interest to quantum engineering. Among the outstanding issues is the nature of the pairing state. A recent surprising discovery is the observation of a resonance in the spin excitation spectrum at an antiferromagnetic wavevector [C. Duan *et al.*, Nature **600**, 636 (2021)], which stands in apparent contrast to the ferromagnetic nature of the interactions expected in this system. We show how the puzzle can be resolved by a multiorbital spin-triplet pairing constructed from local degrees of freedom. Because it does not commute with the kinetic part of the Hamiltonian, the pairing contains both intra- and inter- band terms in the band basis. We demonstrate that the intraband pairing component naturally yields a spin resonance at the antiferromagnetic wavevector. Our work illustrates how orbital degrees of freedom can enrich the nature and properties of spin-triplet superconductivity of strongly-correlated quantum materials.

*Introduction.* The uranium-based dichalcogenide $UTe_2$ is a prime candidate for spin-triplet superconductors [1–10]. Because spin-triplet pairing [11–14] can lead to topological states that host Majorana fermions, which represent a promising route towards fault tolerant quantum computing [15], this system is of extensive current interest. $UTe_2$ transitions to a superconducting state below $T_c = 1.6$ K. It has a strongly-correlated paramagnetic normal state, with a Kondo temperature of about 70 K marking the onset of heavy-fermion behavior such as a highly enhanced effective mass [16]. Evidence for the spin-triplet superconductivity includes the nearly constant Knight shift as observed in nuclear magnetic resonance (NMR) measurements [1, 4, 10] across $T_c$, large upper critical fields exceeding the Pauli limit [1], and indications of chiral edge states from scanning tunneling microscopy (STM) experiments [8]. There is also evidence of time-reversal symmetry breaking from a non-zero polar Kerr effect [9]. Analogy with the uranium-based heavy-fermion superconductors $UGe_2$, URhGe and UCoGe [17–19] suggests the natural possibility that ferromagnetic (FM) spin correlations are important for superconductivity in $UTe_2$. Early evidence for the role of FM correlations in the normal state comes from the enhanced bulk magnetic susceptibility [1] as well as by $\mu$SR measurements [7]. Still, the nature of the pairing state remains enigmatic [20–25].

Recently, several experiments [26–31] have suggested the presence of antiferromagnetic (AF) spin correlations in $UTe_2$. The inelastic neutron scattering (INS) experiments reveal spin fluctuations at an AF wavevector, a feature that has been attributed to the Ruderman-Kittel-Kasuya-Yosida (RKKY) interactions between the U $5f$ electrons [27]. Strikingly, measurements below $T_c$ have uncovered a spin resonance near the AF wavevector [30, 31]. The observation of an AF spin resonance came as a surprise, since it has typically been associated with spin-singlet pairing [32–35]. In the spin-singlet pairing case, the spin resonance has, quite extensively, been attributed to collective excitations of a particle-hole spin composite, at a wave vector that connects parts of the Fermi surfaces with a sign change in the superconducting order parameter ($\Delta_k = -\Delta_{k+q}$) [34, 36–38]. In the case of $UTe_2$, the central new questions are two-fold: how does spin-triplet pairing develop when the overall magnetic fluctuations are AF, and how does the spin-triplet pairing in turn lead to an AF spin resonance?

In this work, we advance a resolution to these seemingly contradictory issues. The key idea, alluded to by some of us in Ref. 30 and developed here, is that pairing in the strongly-correlated (heavy-fermion) system $UTe_2$ is to be constructed in terms of its multiple local degrees of freedom that we refer to as orbitals; these include the sublattice degrees of freedom associated with different U-sites in a unit cell. As a result, the spin-triplet pairing is a matrix not only in spin space but also in orbital space. Reminiscent of a nontrivial class of multi-orbital spin-singlet pairing states [39–42], the pairing matrix does not commute with the kinetic part of the Hamiltonian. This in turn implies that, in the band basis, the pairing matrix contains both intra- and inter-band pairing components. We show that, while the overall pairing matrix has the spin-triplet odd-parity form, the intraband pairing component gives rise to a spin resonance. We achieve an understanding of the spin dynamics at the proof-of-principle level, leaving more quantitative analyses for future studies. We note in passing that the interplay between AF correlations and spin-triplet pairing is potentially relevant to other heavy-fermion superconductors, including the venerable case of $UPt_3$ [43–45] and the more recently-discussed quantum critical systems [46–48].

*Competing magnetic interactions and microscopic Hamiltonian.* $UTe_2$ crystallizes in an orthorhombic, centrosymmetric structure, with space group 71 ($Immm$) and two $U$ atoms per unit cell. Electronic-structure calculations [27, 49, 50], core-level photoelectron spectroscopy [51, 52] and the spin size extracted by inelastic neutron scattering [30] are consistent with the U $5f$ electrons in a doublet of predominantly $j = 5/2$, with $m_j = \pm 1/2$.

We thus consider two Kramers doublets per unit cell. The effective interactions are labeled by $J_i$'s ($i = 1 - 4$) in

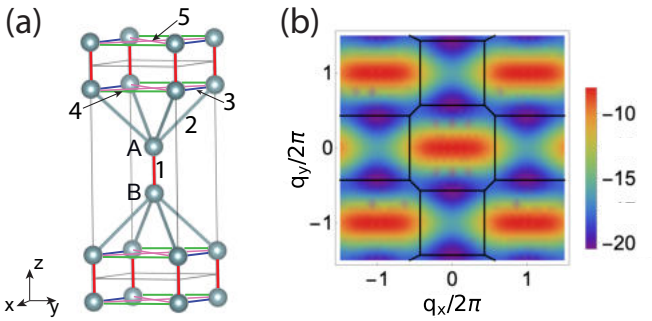


FIG. 1. (a) The structure of $UTe_2$. The numbers label the bonds for the exchange interactions and kinetic parameters. The black thin lines mark the conventional unit cell, which contains two primitive cells. (b) The exchange interaction eigenvalue, $J_-(\boldsymbol{q})$, plotted within the $(q_x, q_y)$ plane for $q_z = 0$. It is the most negative around the AF wavevector, $\boldsymbol{q} \sim \mathbf{Q}$. The color bar marks the values in meV.

Fig. 1(a). We take the exchange interactions to be

$$H_J = -\sum_i I^\mu S^\mu_{i,A} S^\mu_{i,B} + \sum_{ir,mn} J_r \boldsymbol{S}_{i,m} \cdot \boldsymbol{S}_{i+r,n}. \quad (1)$$

Here, $A/B$ labels the two sublattices [Fig. 1(a)], $i$ marks a unit cell and $S^\mu$ is a component of the local spin for $\mu = x, y, z$. Due to the special role that the intra-"dimer" exchange interaction plays, we refer to $J^\mu_1$ as $-I^\mu$. In addition, $J_r$ ($r \geq 2$) labels the $r$th-nearest neighbor exchange interaction that connects $m$ and $n$ sublattices [Fig. 1(a)]. We expect to have significant $\mu$-dependence due to the large spin-orbit coupling (SOC) that is inherent to the $5f$-electrons of U-ions. The effect of this spin anisotropy is evidenced by magnetic susceptibility measurements [1, 53]. In our analysis, only the spin anisotropy of $J_1 = -I$ will be important and kept track of. In practice, we consider $r$ up to 4 and have

$$H_J = \sum_{\boldsymbol{q}} \begin{pmatrix} \boldsymbol{S}_{\boldsymbol{q},A} & \boldsymbol{S}_{\boldsymbol{q},B} \end{pmatrix} J(\boldsymbol{q}) \begin{pmatrix} \boldsymbol{S}_{-\boldsymbol{q},A} \\ \boldsymbol{S}_{-\boldsymbol{q},B} \end{pmatrix} \quad (2)$$

with

$$\begin{aligned} J(\boldsymbol{q}) =& [2\, J_3\, T_3(\boldsymbol{q}) + 2\, J_4\, T_4(\boldsymbol{q})]\, \tau_0 \\ &+ [-I + 4\, J_2\, T_{2,1}(\boldsymbol{q})]\, \tau_x + 4\, J_2\, T_{2,2}(\boldsymbol{q})\, \tau_y, \end{aligned} \quad (3)$$

where the Pauli matrices $\tau_i$ are defined in the orbital space, while $T_{2,1}(\boldsymbol{q}) = \cos(q_x/2)\cos(q_y/2)\cos(q_z/2)$, $T_{2,2}(\boldsymbol{q}) = \cos(q_x/2)\cos(q_y/2)\sin(q_z/2)$, $T_3(\boldsymbol{q}) = \cos(q_x)$, and $T_4(\boldsymbol{q}) = \cos(q_y)$. The INS experiments [28, 30] allow for the inference of FM $I$ and $J_3$ and AF $J_2$ and $J_4$ (see Supplementary Materials).

The U-U distance within a dimer is smaller than all the other U-U distances, and we expect $I$ to be the strongest. We have performed first-principles calculations within density functional theory [54] (see also Ref. 21). Our calculations give average values of $-J_1 \equiv I \lesssim 20$ meV and $J_2 \sim 0.75$ meV. Estimates of $J_{3,4}$ are more demanding as they require a larger unit cell with five magnetic configurations considered on an equal footing. Based on these results and the Kondo temperature scale, we set $I^x = 15$ meV, $J_2 = 1$ meV, $J_3 = -0.5$ meV, and $J_4 = 2$ meV. The largest negative eigenvalue of the exchange interaction matrix is:

$$J_-(\boldsymbol{q}) = -I + 4J_2 \cos\frac{q_x}{2}\cos\frac{q_y}{2} + 2J_3 \cos q_x + 2J_4 \cos q_y\,, \quad (4)$$

for $q_z = 0$. Importantly, the ferromagnetic intra-dimer interaction $J_1 \equiv -I$ is featureless in wavevector space. Instead, the inter-unit-cell AF interactions are responsible for the minimum of $J_-(\boldsymbol{q})$ near $\boldsymbol{q} \sim \mathbf{Q} = (0, \pi)$, as shown in Fig. 1(b).

The Hamiltonian is that of a Kondo lattice, with the $5f$-electrons occupying $\Gamma_5$ Kramers doublets on the U sites that are Kondo-coupled to the *spd*-electrons and, in addition, interact with each other through $H_J$. For our proof-of-principle purpose, we adopt an effective description that is based exclusively on effective $f$-electrons and incorporate $H_J$ and a kinetic part $H_{kin}$ (see below).

*Spin-triplet pairing – orbital basis.* The strongly-correlated nature of the $5f$ electrons suggests the construction of pairing based on the local degrees of freedom [30]. Given that the FM intra-dimer interaction $I$ is the strongest, we consider the dominant pairing to be between the $5f$ electrons on a dimer, as introduced in Ref. 23 and subsequently in Ref. 24. An odd-parity pairing can be constructed in terms of two fermions with opposite parity [the even and odd parity combinations of the fermions at the $A$ and $B$ sites, $c_{e/o} = (c_A \pm c_B)/\sqrt{2}$, where $c_e$ ($c_o$) is even (odd)] and are, equivalently, written as follows:

$$\begin{aligned} \Delta_x &= \delta_x \tau_y \otimes \sigma_x \otimes \gamma_1 \\ \Delta_y &= \delta_y \tau_y \otimes \sigma_y \otimes \gamma_1 \\ \Delta_z &= \delta_z \tau_y \otimes \sigma_z \otimes \gamma_1\,. \end{aligned} \quad (5)$$

Here, $\delta_x, \delta_y, \delta_z$ denote the pairing amplitudes whereas $\sigma_i$ and $\gamma_i$ are respectively Pauli matrices in spin and Nambu spaces. A generic spin triplet pairing can be characterized by the vector $\vec{d} = (\delta_x, \delta_y, \delta_z)$.

In $UTe_2$, the magnetic susceptibility shows extreme anisotropy [1]. In the normal state, the magnetic susceptibilities satisfy $\chi_x \gg \chi_z > \chi_y$, which is consistent with the hierarchy of exchange interaction, $I^x \gg I^z > I^y$. In a triplet superconductor, the direction of the dominant exchange interaction promotes superconducting pairing with a perpendicular spin component [55] (see Supplementary Materials). Accordingly, the energetically favored pairing component is the $\Delta_y$ channel in the $B_{3u}$ irreducible representation of the $D_{2h}$ point group. We denote its overall amplitude to be $\delta$, and set $\delta_x = \delta_z = 0$; extension to including these other pairing channels is discussed below.

*Spin-triplet pairing – band basis.* The Bogoliubov de Gennes (BdG) Hamiltonian is now written as

$$H = \sum_{\boldsymbol{k}} \Psi^\dagger_{\boldsymbol{k}} \left[\, H_{kin}(\boldsymbol{k}) + \Delta(\boldsymbol{k}) \,\right] \Psi_{\boldsymbol{k}}\,, \quad (6)$$

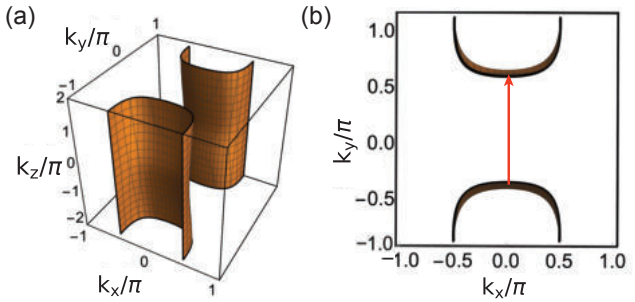


FIG. 2. (a) The 3D Fermi surface and (b) the corresponding top view, with the spanning wavevector (red arrow) that is close to **Q**.

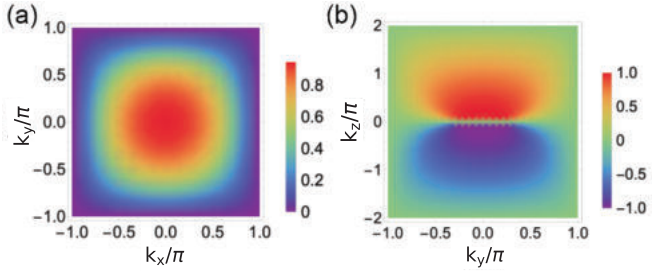


FIG. 3. Schematic illustration of the intraband pairing $(d_1(\boldsymbol{k})/\delta)$ within (a) the $k_z = \pi$-plane and (b) the $k_x = 0$-plane.

where $\Psi^\dagger_{\boldsymbol{k}} = \left(c^\dagger_{\boldsymbol{k},m,\sigma}, c_{-\boldsymbol{k},n,\sigma'}(i\sigma_y)\right)$ is the Nambu spinor, and $m, n = A/B$ are the orbital (sublattice) indices.

We incorporate the hopping terms $t_r$ following the same numbering scheme of the bonds as for the exchange interactions, and also allow for $t_5$ defined on the diagonal counterpart of the bonds 3 and 4 [c.f., Fig. 1(a)]. The kinetic part then has the following form

$$H_{kin} = \sum_i t_1 c^\dagger_{i,A} c_{i,B} + \sum_{ir,mn} t_r c^\dagger_{i,m} c_{i+r,n}. \tag{7}$$

In momentum space (see Supplementary Materials for the definition of Fourier transformation), $H_{kin}$ becomes:

$$\begin{aligned} H_{kin}(\boldsymbol{k}) =& \xi_0(\boldsymbol{k})\,\tau_0 + \xi_x(\boldsymbol{k})\,\tau_x + \xi_y(\boldsymbol{k})\,\tau_y \\ =& [2\,t_3\,T_3(\boldsymbol{k}) + 2\,t_4\,T_4(\boldsymbol{k}) + 4\,t_5\,T_5(\boldsymbol{k})]\,\tau_0 \\ &+ [t_1 + 4\,t_2\,T_{2,1}(\boldsymbol{k})]\,\tau_x + 4\,t_2\,T_{2,2}(\boldsymbol{k})\,\tau_y\,, \end{aligned} \tag{8}$$

where $\sigma_i$ are the usual Pauli matrices in spin space, and $T_5(\boldsymbol{k}) = \cos(k_x)\cos(k_y)$. We note that $\xi_{0,x}(\boldsymbol{k}) = \xi_{0,x}(-\boldsymbol{k})$ and $\xi_y(\boldsymbol{k}) = -\xi_y(-\boldsymbol{k})$. Guided by the DMFT calculations of the electronic structure [27, 56] and the Kondo temperature, we take $t_1 = -0.95$ meV, $4t_2 = 1$ meV, $2t_3 = -2$ meV, $2t_4 = 2$ meV, $4t_5 = 6$ meV, and a chemical potential $\mu = 3$ meV. The Fermi surface is shown in Fig. 2(a,b), which has a quasi- two-dimensional (2D) shape with a Fermi pocket surrounding the $(0, \pi, k_z)$ line. [A suitable variation in $\mu$ can lead to the coexistence of another Fermi pocket surrounding the $(\pi, 0, k_z)$ line.] For these parameters, the total bandwidth is $W = 19$ meV; it is comparable to the strength of the exchange interaction [c.f., Fig. 1(b)], and each is about the Kondo temperature up to the typical conversion factor from temperature to energy (roughly 3).

We can now project the pairing onto the band basis. Given that the kinetic and pairing parts do not commute with each other, the two cannot be simultaneously diagonalized. The pairing part must contain both intra and interband components. To see this, we first introduce a transformation that diagonalizes the kinetic energy:

$$U^\dagger_{\boldsymbol{k}} H_{kin}(\boldsymbol{k}) U_{\boldsymbol{k}} = \begin{pmatrix} \epsilon_-(\boldsymbol{k}) & 0 \\ 0 & \epsilon_+(\boldsymbol{k}) \end{pmatrix} \otimes \sigma_0 \tag{9}$$

where the band energy $\epsilon_\pm(\boldsymbol{k}) = \xi_0 \pm \sqrt{\xi_x^2 + \xi_y^2}$. The explicit form of $U_{\boldsymbol{k}}$ is given in the Supplemental Materials. The pairing in the band basis takes the form

$$\Delta(\boldsymbol{k}) = U^\dagger_{\boldsymbol{k}} \Delta_y U_{-\boldsymbol{k}} = d_1(\boldsymbol{k})\alpha_3 \otimes \sigma_2 + d_2(\boldsymbol{k})\alpha_2 \otimes \sigma_2\,. \tag{10}$$

Here, $\alpha_2$ and $\alpha_3$ are Pauli matrices in the band basis, and the associated inter- and intra- band pairing components are:

$$\begin{aligned} d_1(\boldsymbol{k}) =& \delta\,\xi_y(\boldsymbol{k})/\sqrt{\xi_x^2(\boldsymbol{k}) + \xi_y^2(\boldsymbol{k})}, \\ d_2(\boldsymbol{k}) =& \delta\,\xi_x(\boldsymbol{k})/\sqrt{\xi_x^2(\boldsymbol{k}) + \xi_y^2(\boldsymbol{k})}\,. \end{aligned} \tag{11}$$

The band-diagonal $\alpha_3$ and band-off-diagonal $\alpha_2$ pairing components have $p_z$ and $s$ form factors, respectively. As illustrated in Fig, 3, the intraband gap functions vanish in the $k_z = 0, \pm 2\pi$ plane.

The full BdG spectrum can be obtained by diagonalizing Eq. 6 (see Supplemental Materials), which yields

$$\begin{aligned} &E_\pm(\boldsymbol{k}) \\ &= \sqrt{\left(\sqrt{\xi_0^2(\boldsymbol{k}) + \delta^2 \sin^2\phi(\boldsymbol{k})} \pm B(\boldsymbol{k})\right)^2 + \delta^2(1 - \sin^2\phi(\boldsymbol{k}))} \end{aligned} \tag{12}$$

with $B(\boldsymbol{k}) = \sqrt{\xi_x^2(\boldsymbol{k}) + \xi_y^2(\boldsymbol{k})}$, and $\sin\phi(\boldsymbol{k}) = \frac{\xi_x(\boldsymbol{k})}{B(\boldsymbol{k})}$. On the Fermi surface, $\xi_0^2(\boldsymbol{k}) = \xi_x^2(\boldsymbol{k}) + \xi_y^2(\boldsymbol{k})$, and there is a full gap. This feature can be modified when the other spin-triplet pairing components are included (see below), but our conclusion about the AF spin-resonance will be robust.

*Spin-triplet pairing and spin resonance.* The orbital-dependent spin susceptibility is given by

$$\chi_{\alpha\gamma}(\boldsymbol{q}, i\omega) = \sum_\lambda [\chi^0(\boldsymbol{q}, i\omega)]_{\alpha\lambda} [\mathbb{I} + J(\boldsymbol{q})[\chi^0(\boldsymbol{q}, i\omega)]]^{-1}_{\lambda\gamma}, \tag{13}$$

where $\alpha$, $\beta$, $\gamma$ and $\lambda$ denote the orbitals. For $q_z = 0$ of our interest, the total spin susceptibility is given by

$$\chi^\mu(\boldsymbol{q}) = 2[\chi^\mu_{AA}(\boldsymbol{q}) + \chi^\mu_{AB}(\boldsymbol{q})]\,. \tag{14}$$

As noted before, $\mu = x, y, z$ denotes the spin directions.

Unlike singlet superconducting states, here $\chi^\parallel$ and $\chi^\perp$, the spin susceptibility parallel and perpendicular to the $\vec{d}$ vector

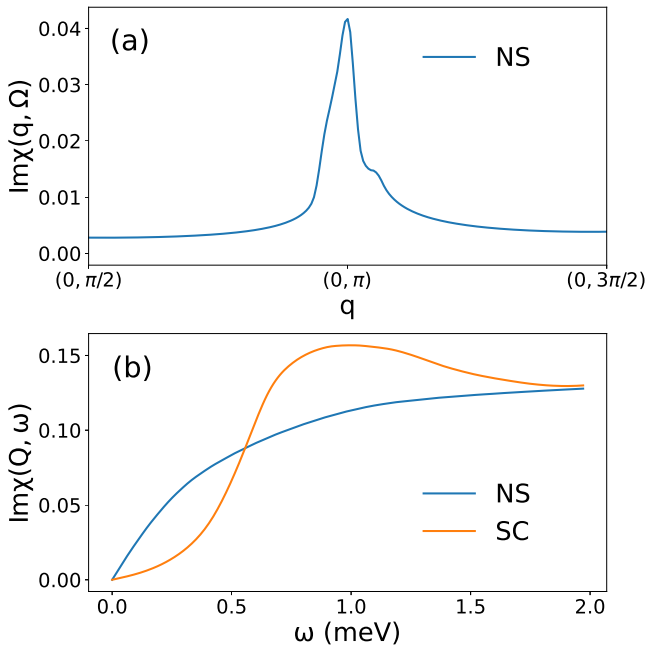


FIG. 4. (a) The imaginary part of the dynamical spin susceptibility v.s. $q$ in the normal state (NS) with frequency $\omega = 0.25\text{meV}$ and (b) of the dynamical spin susceptibility in both the superconducting states (SC) and normal states, at $\mathbf{Q} = (0, \pi)$, as a function of frequency ($\omega$, normalized by $\Delta$, the maximal pairing gap on the Fermi surface).

respectively, have different superconducting coherence factors [57, 58] (see Supplementary Materials). Because of the highly anisotropic nature of the exchange interaction $I$, the dominating susceptibility is along the $\mu = x$ direction, for which we can expect a coherence factor favoring a spin resonance to be of the same sign at $\boldsymbol{k}$ and $\boldsymbol{k}+\mathbf{Q}$. We will therefore calculate $\chi^x$ in the following (unless otherwise specified).

We are now in position to present our results on the spin dynamics. We first consider the results for the normal state (NS), obtained from Eq. 14 with $\delta = 0$. Fig. 4(a) shows the $\boldsymbol{q}$-dependence of the imaginary part of the dynamical spin susceptibility at a fixed $\omega = 0.21$ meV, along a momentum path from $(0, \frac{\pi}{2})$ to $(0, \frac{3\pi}{2})$. It exhibits an AF peak at wavevectors around $\mathbf{Q} = (0, \pi)$, which is near where $J_-(\boldsymbol{q})$ is the most negative and also is close to connecting the Fermi sheets.

In the superconducting phase, we first solve the pairing function self-consistently to show the development of spin-triplet pairing. This is described in the Supplementary Materials, where we indeed find the $\Delta_y$ pairing. With the model parameters described earlier, the maximal value of the gap close to the Fermi surface is found to be $\Delta = 0.44\text{meV}$.

Fig. 4(b) shows the energy dependence of $\text{Im}\chi(\mathbf{Q}, \omega)$, the imaginary part of the $J(\boldsymbol{q})$-enhanced dynamical spin susceptibility at the wavevector $\mathbf{Q} = (0, \pi)$, in the superconducting state. (The bare dynamical spin susceptibility is given in the Supplementary Materials.) A spin resonance is clearly seen around $\omega_{res} \approx 1$ meV. The resonance can be regarded as a collective excitation from single-particle and single-hole states, for all the different $k_z$, that are located across the $q_y$ direction. The $k_z$ variation of the intraband pairing component [Fig. 3(b)] contributes to the broadening of the resonance.

One of our main conclusions is the existence of a spin resonance at the AF wavevector. We find the ratio $\omega_{res}/\Delta$ to be larger than what is typical (that is significantly less than 2) for the usual quasi-2D (spin-singlet) superconductors [38]. However, the precise value of this ratio depends on details of the interactions and Fermi surface.

Our results naturally provide an overall understanding of the salient experimental-motivated issues outline earlier. First, the calculated dynamical spin susceptibility in the normal state [Fig. 4(a)] realizes the AF fluctuations that have been observed by INS experiments [27, 28]. This is further illustrated in Fig. 5 (Supplementary Materials), where the theoretically determined $\boldsymbol{q}$-structure is shown to be comparable with the momentum pattern observed experimentally. Second, by incorporating the underlying local degrees of freedom, we have shown that such AF correlations promote the experimentally-evidenced spin-triplet pairing. Third, we have demonstrated that the spin-triplet pairing gives rise to an AF spin resonance. Our results [Fig. 4(b)] capture the salient features of the experimental observation, as illustrated in the Supplementary Materials (Fig. 6). Finally, the SOC-induced spin-anisotropic interactions built into our model capture the feature that the dominant magnetic fluctuations appear in the $x$-direction, as observed in the INS measurements [30].

*Discussion.* Several remarks are in order. First, the importance of the local degrees of freedom and the associated multiorbital form of spin-triplet pairing reflect the underlying strong correlations of the system and are to be contrasted with weak-coupling approaches.

Second, a main focus of our work is a proof-of-principle demonstration that, when multiorbital pairing is considered, the spin-triplet nature of the superconducting state in $\text{UTe}_2$ can naturally be reconciled with the AF correlations in the normal state and the emergence of an AF spin resonance in the superconducting state. This sets the stage for extensions of the model. For example, the pairing function can be generalized to the non-unitary case, which can i) break the time-reversal symmetry; and ii) lead to a BdG spectrum that not only depends on the usual $|\vec{d}|^2$ gap term, but also on an additional splitting proportional to $|i\vec{d}^* \times \vec{d}|$ [59]. While the nodal structure of the pairing state will be affected, the linkage between the spin-triplet pairing and AF spin resonance is expected to be robust. In the same vein, our work also sets the stage for addressing the quantitative aspects of the spin resonance, such as the resonance energy versus the superconducting pairing gap. For the latter, we note that the multiplicity of the $5f$ electrons in $\text{UTe}_2$ may well lead to orbital-selective correlations, as has been observed in other U-based heavy-fermion systems [60, 61]. Thus, there could very well be multiple pairing gaps that remain to be experimentally probed.

Third, the matrix form for the spin-triplet pairing we have considered bears some conceptual similarity to its spin-singlet

counterpart in the contexts of both the iron-based superconductors [39, 40] and $CeCu_2Si_2$ [41, 42, 62]. Our work therefore highlights the notion that the emerging conceptual framework for multiorbital superconducting pairing, which is anchored by the iron-based superconductors [63–66], may apply to a variety of correlated systems.

*Conclusion.* To summarize, we have highlighted the importance of the matrix structure associated with the local degrees of freedom of the heavy-fermion superconductor $UTe_2$. This structure allows us to provide a natural understanding of some outstanding issues that have been raised for this system. The puzzling questions include how spin-triplet pairing can develop when the overall magnetic fluctuations are antiferromagnetic, and how the spin-triplet pairing can in turn lead to an antiferromagnetic spin resonance. In our theory, the spin-triplet pairing is enabled by the dominant intra-dimer ferromagnetic interactions along with the inter-unit-cell antiferromagnetic interactions. The latter not only are responsible for the observed antiferromagnetic fluctuations but also make them react to the onset of superconductivity. We expect that the new insight our work reveals, *viz.* the local degrees of freedom can qualitatively enrich the nature and properties of spin-triplet superconductivity, will be relevant to a variety of other strongly-correlated quantum materials.

*Acknowledgement.*— We thank Ryan Baumbach, Nick Butch, Sheng Ran, Brian Maple, Chandan Setty, Yi-feng Yang and, particularly, Pengcheng Dai and Chunruo Duan for useful discussions. Work at Rice was primarily supported by the U.S. Department of Energy, Office of Science, Basic Energy Sciences, under Award No. DE-SC0018197 and additionally supported by the Robert A. Welch Foundation Grant No. C-1411. The majority of the computational calculations have been performed on the Shared University Grid at Rice funded by NSF under Grant EIA-0216467, a partnership between Rice University, Sun Microsystems, and Sigma Solutions, Inc., the Big-Data Private-Cloud Research Cyberinfrastructure MRI-award funded by NSF under Grant No. CNS-1338099 and by Rice University, and the Extreme Science and Engineering Discovery Environment (XSEDE) by NSF under Grant No. DMR160057. Work at Los Alamos was supported by LANL LDRD Program, UC Laboratory Fees Research Program (Grant Number: LFR-20-653926), and in part by Center for Integrated Nanotechnologies. One of us (Q.S.) acknowledges the hospitality of the Aspen Center for Physics, which is supported by NSF grant No. PHY-1607611.

⊕ These authors contributed equally to this work.

[1] S. Ran, C. Eckberg, Q.-P. Ding, Y. Furukawa, T. Metz, S. R. Saha, I.-L. Liu, M. Zic, H. Kim, J. Paglione, and N. P. Butch, Science **365**, 684 (2019).
[2] D. Aoki, A. Nakamura, F. Honda, D. Li, Y. Homma, Y. Shimizu, Y. J. Sato, G. Knebel, J.-P. Brison, A. Pourret, D. Braithwaite, G. Lapertot, Q. Niu, M. Vališka, H. Harima, and J. Flouquet, Journal of the Physical Society of Japan **88**, 043702 (2019).
[3] S. Ran, I.-L. Liu, Y. S. Eo, D. J. Campbell, P. M. Neves, W. T. Fuhrman, S. R. Saha, C. Eckberg, H. Kim, D. Graf, F. Balakirev, J. Singleton, J. Paglione, and N. P. Butch, Nature Physics **15**, 1250 (2019).
[4] Y. Tokunaga, H. Sakai, S. Kambe, T. Hattori, N. Higa, G. Nakamine, S. Kitagawa, K. Ishida, A. Nakamura, Y. Shimizu, Y. Homma, D. Li, F. Honda, and D. Aoki, Journal of the Physical Society of Japan **88**, 073701 (2019).
[5] G. Knebel, W. Knafo, A. Pourret, Q. Niu, M. Vališka, D. Braithwaite, G. Lapertot, M. Nardone, A. Zitouni, S. Mishra, I. Sheikin, G. Seyfarth, J.-P. Brison, D. Aoki, and J. Flouquet, Journal of the Physical Society of Japan **88**, 063707 (2019).
[6] T. Metz, S. Bae, S. Ran, I.-L. Liu, Y. S. Eo, W. T. Fuhrman, D. F. Agterberg, S. M. Anlage, N. P. Butch, and J. Paglione, Phys. Rev. B **100**, 220504 (2019).
[7] S. Sundar, S. Gheidi, K. Akintola, A. M. Côté, S. R. Dunsiger, S. Ran, N. P. Butch, S. R. Saha, J. Paglione, and J. E. Sonier, Phys. Rev. B **100**, 140502 (2019).
[8] L. Jiao, S. Howard, S. Ran, Z. Wang, J. O. Rodriguez, M. Sigrist, Z. Wang, N. P. Butch, and V. Madhavan, Nature **579**, 523 (2020).
[9] I. M. Hayes, D. S. Wei, T. Metz, J. Zhang, Y. S. Eo, S. Ran, S. R. Saha, J. Collini, N. P. Butch, D. F. Agterberg, A. Kapitulnik, and J. Paglione, Science , eabb0272 (2021).
[10] G. Nakamine, K. Kinjo, S. Kitagawa, K. Ishida, Y. Tokunaga, H. Sakai, S. Kambe, A. Nakamura, Y. Shimizu, Y. Homma, D. Li, F. Honda, and D. Aoki, Phys. Rev. B **103**, L100503 (2021).
[11] T. M. Rice and M. Sigrist, Journal of Physics: Condensed Matter **7**, L643 (1995).
[12] C. Kallin and A. J. Berlinsky, Journal of Physics: Condensed Matter **21**, 164210 (2009).
[13] A. Ramires and M. Sigrist, Phys. Rev. B **100**, 104501 (2019).
[14] W. Huang, Y. Zhou, and H. Yao, Phys. Rev. B **100**, 134506 (2019).
[15] C. Nayak, S. H. Simon, A. Stern, M. Freedman, and S. Das Sarma, Rev. Mod. Phys. **80**, 1083 (2008).
[16] S. Kirchner, S. Paschen, Q. Chen, S. Wirth, D. Feng, J. D. Thompson, and Q. Si, Rev. Mod. Phys. **92**, 011002 (2020).
[17] S. S. Saxena, P. Agarwal, K. Ahilan, F. M. Grosche, R. K. W. Haselwimmer, M. J. Steiner, E. Pugh, I. R. Walker, S. R. Julian, P. Monthoux, G. G. Lonzarich, A. Huxley, I. Sheikin, D. Braithwaite, and J. Flouquet, Nature **406**, 587 (2000).
[18] D. Aoki, A. Huxley, E. Ressouche, D. Braithwaite, J. Flouquet, J.-P. Brison, E. Lhotel, and C. Paulsen, Nature **413**, 613 (2001).
[19] N. T. Huy, A. Gasparini, D. E. de Nijs, Y. Huang, J. C. P. Klaasse, T. Gortenmulder, A. de Visser, A. Hamann, T. Görlach, and H. v. Löhneysen, Phys. Rev. Lett. **99**, 067006 (2007).
[20] J. Ishizuka, S. Sumita, A. Daido, and Y. Yanase, Phys. Rev. Lett. **123**, 217001 (2019).
[21] Y. Xu, Y. Sheng, and Y.-f. Yang, Phys. Rev. Lett. **123**, 217002 (2019).
[22] A. H. Nevidomskyy, arXiv preprint arXiv:2001.02699 (2020).
[23] H. Hu and Q. Si, Talk given at Fundamentals of Quantum Materials Workshop on Superconductivity of $UTe_2$, January 10 (2020).
[24] T. Shishidou, H. G. Suh, P. M. R. Brydon, M. Weinert, and D. F. Agterberg, Phys. Rev. B **103**, 104504 (2021).
[25] A. Kreisel, Y. Quan, and P. Hirschfeld, arXiv preprint arXiv:2110.14624 (2021).
[26] S. M. Thomas, F. B. Santos, M. H. Christensen, T. Asaba,

F. Ronning, J. D. Thompson, E. D. Bauer, R. M. Fernandes, G. Fabbris, and P. F. S. Rosa, Science Advances **6**, eabc8709, publisher: American Association for the Advancement of Science.
[27] C. Duan, K. Sasmal, M. B. Maple, A. Podlesnyak, J.-X. Zhu, Q. Si, and P. Dai, Phys. Rev. Lett. **125**, 237003 (2020).
[28] W. Knafo, G. Knebel, P. Steffens, K. Kaneko, A. Rosuel, J.-P. Brison, J. Flouquet, D. Aoki, G. Lapertot, and S. Raymond, Phys. Rev. B **104**, L100409 (2021).
[29] N. P. Butch, S. Ran, S. R. Saha, P. M. Neves, M. P. Zic, J. Paglione, S. Gladchenko, Q. Ye, and J. A. Rodriguez, arXiv preprint arXiv:2112.12267 (2021).
[30] C. Duan, R. E. Baumbach, A. Podlesnyak, Y. Deng, C. Moir, A. J. Breindel, M. B. Maple, E. M. Nica, Q. Si, and P. Dai, Nature **600**, 636 (2021).
[31] S. Raymond, W. Knafo, G. Knebel, K. Kaneko, J.-P. Brison, J. Flouquet, D. Aoki, and G. Lapertot, Journal of the Physical Society of Japan **90**, 113706 (2021).
[32] J. Rossat-Mignod, L. P. Regnault, C. Vettier, P. Bourges, P. Burlet, J. Bossy, J. Y. Henry, and G. Lapertot, Physica C: Superconductivity **185-189**, 86 (1991).
[33] H. A. Mook, M. Yethiraj, G. Aeppli, T. E. Mason, and T. Armstrong, Phys. Rev. Lett. **70**, 3490 (1993).
[34] H. F. Fong, B. Keimer, P. W. Anderson, D. Reznik, F. Doğan, and I. A. Aksay, Phys. Rev. Lett. **75**, 316 (1995).
[35] P. Dai, Rev. Mod. Phys. **87**, 855 (2015).
[36] D. Z. Liu, Y. Zha, and K. Levin, Phys. Rev. Lett. **75**, 4130 (1995).
[37] Y. Zha, K. Levin, and Q. Si, Phys. Rev. B **47**, 9124 (1993).
[38] M. Eschrig, Advances in Physics **55**, 47 (2006).
[39] E. M. Nica, R. Yu, and Q. Si, npj Quantum Materials **2**, 24 (2017).
[40] E. M. Nica and Q. Si, npj Quantum Materials **6**, 3 (2021).
[41] G. M. Pang, M. Smidman, J. L. Zhang, L. Jiao, Z. F. Weng, E. M. Nica, Y. Chen, W. B. Jiang, Y. J. Zhang, W. Xie, H. S. Jeevan, H. Lee, P. Gegenwart, F. Steglich, Q. Si, and H. Q. Yuan, Proc. Natl. Acad. Sci. U.S.A. (2018), 10.1073/pnas.1720291115.
[42] M. Smidman, O. Stockert, J. Arndt, G. M. Pang, L. Jiao, H. Q. Yuan, H. A. Vieyra, S. Kitagawa, K. Ishida, K. Fujiwara, T. C. Kobayashi, E. Schuberth, M. Tippmann, L. Steinke, S. Lausberg, A. Steppke, M. Brando, H. Pfau, U. Stockert, P. Sun, S. Friedemann, S. Wirth, C. Krellner, S. Kirchner, E. M. Nica, R. Yu, Q. Si, and F. Steglich, Phil. Mag. **98**, 2930 (2018).
[43] G. Aeppli, E. Bucher, C. Broholm, J. K. Kjems, J. Baumann, and J. Hufnagl, Phys. Rev. Lett. **60**, 615 (1988).
[44] J. Sauls, Advances in Physics **43**, 113 (1994).
[45] R. Joynt and L. Taillefer, Rev. Mod. Phys. **74**, 235 (2002).
[46] D. H. Nguyen, A. Sidorenko, M. Taupin, G. Knebel, G. Lapertot, E. Schuberth, and S. Paschen, Nature Communications **12**, 4341 (2021).
[47] H. Hu, A. Cai, L. Chen, and Q. Si, arXiv preprint arXiv:2109.12794 (2021).
[48] J. H. Pixley, L. Deng, K. Ingersent, and Q. Si, Phys. Rev. B **91**, 201109 (2015).
[49] A. B. Shick, S.-i. Fujimori, and W. E. Pickett, Phys. Rev. B **103**, 125136 (2021).
[50] A. B. Shick and W. E. Pickett, Phys. Rev. B **100**, 134502 (2019).
[51] S.-i. Fujimori, I. Kawasaki, Y. Takeda, H. Yamagami, A. Nakamura, Y. Homma, and D. Aoki, Journal of the Physical Society of Japan **90**, 015002 (2021).
[52] S.-i. Fujimori, I. Kawasaki, Y. Takeda, H. Yamagami, A. Nakamura, Y. Homma, and D. Aoki, Journal of the Physical Society of Japan **88**, 103701 (2019).
[53] D. Li, A. Nakamura, F. Honda, Y. J. Sato, Y. Homma, Y. Shimizu, J. Ishizuka, Y. Yanase, G. Knebel, J. Flouquet, and D. Aoki, Journal of the Physical Society of Japan **90**, 073703 (2021).
[54] C. Lane, H. Hu, L. Chen, E. M. Nica, Q. Si, and J.-X. Zhu, in preparation (2021).
[55] A. J. Leggett, Rev. Mod. Phys. **47**, 331 (1975).
[56] L. Miao, S. Liu, Y. Xu, E. C. Kotta, C.-J. Kang, S. Ran, J. Paglione, G. Kotliar, N. P. Butch, J. D. Denlinger, and L. A. Wray, Phys. Rev. Lett. **124**, 076401 (2020).
[57] D. K. Morr, P. F. Trautman, and M. J. Graf, Phys. Rev. Lett. **86**, 5978 (2001).
[58] T. A. Maier and D. J. Scalapino, Phys. Rev. B **78**, 020514 (2008).
[59] M. Sigrist and K. Ueda, Rev. Mod. Phys. **63**, 239 (1991).
[60] Q. Y. Chen, X. B. Luo, D. H. Xie, M. L. Li, X. Y. Ji, R. Zhou, Y. B. Huang, W. Zhang, W. Feng, Y. Zhang, L. Huang, Q. Q. Hao, Q. Liu, X. G. Zhu, Y. Liu, P. Zhang, X. C. Lai, Q. Si, and S. Y. Tan, Phys. Rev. Lett. **123**, 106402 (2019).
[61] I. Giannakis, J. Leshen, M. Kavai, S. Ran, C.-J. Kang, S. R. Saha, Y. Zhao, Z. Xu, J. W. Lynn, L. Miao, L. A. Wray, G. Kotliar, N. P. Butch, and P. Aynajian, Science Advances **5**, eaaw9061 (2019).
[62] A. Amorese, A. Marino, M. Sundermann, K. Chen, Z. Hu, T. Willers, F. Choueikani, P. Ohresser, J. Herrero-Martin, S. Agrestini, C.-T. Chen, H.-J. Lin, M. W. Haverkort, S. Seiro, C. Geibel, F. Steglich, L. H. Tjeng, G. Zwicknagl, and A. Severing, Phys. Rev. B **102**, 245146 (2020).
[63] R. Yu, J.-X. Zhu, and Q. Si, Phys. Rev. B **89**, 024509 (2014).
[64] Z. P. Yin, K. Haule, and G. Kotliar, Nature Physics **10**, 845 (2014).
[65] T. Ong, P. Coleman, and J. Schmalian, Proc. Nat. Acad. Sci. **113**, 5486 (2016).
[66] Q. Si, R. Yu, and E. Abrahams, Nat. Rev. Mater. **1**, 16017 (2016).

## SUPPLEMENTARY MATERIALS

### COMPARING OUR RESULTS WITH INS EXPERIMENTS

In this section, we compare our theoretical results with the INS measurements of Ref. [30]. One comparison is in the momentum domain. As shown in Fig. 5(a) [i.e., Fig. 1(b) of the main text], the minima of the exchange interaction are located about the same positions where the AF spin excitations are observed in the INS experiments: They appear at BZ boundaries along the $q_y$ direction, as marked by the red ellipses in Fig. 5(b) [30].

The other comparison is in the frequency domain. The spin resonance from our calculations in the superconducting state, presented in Fig. 6(a) [i.e., Fig. 4(b) of the main text], captures the basic features of the spin resonance observed in the INS experiments, which is displayed in Fig. 6(b) [30].

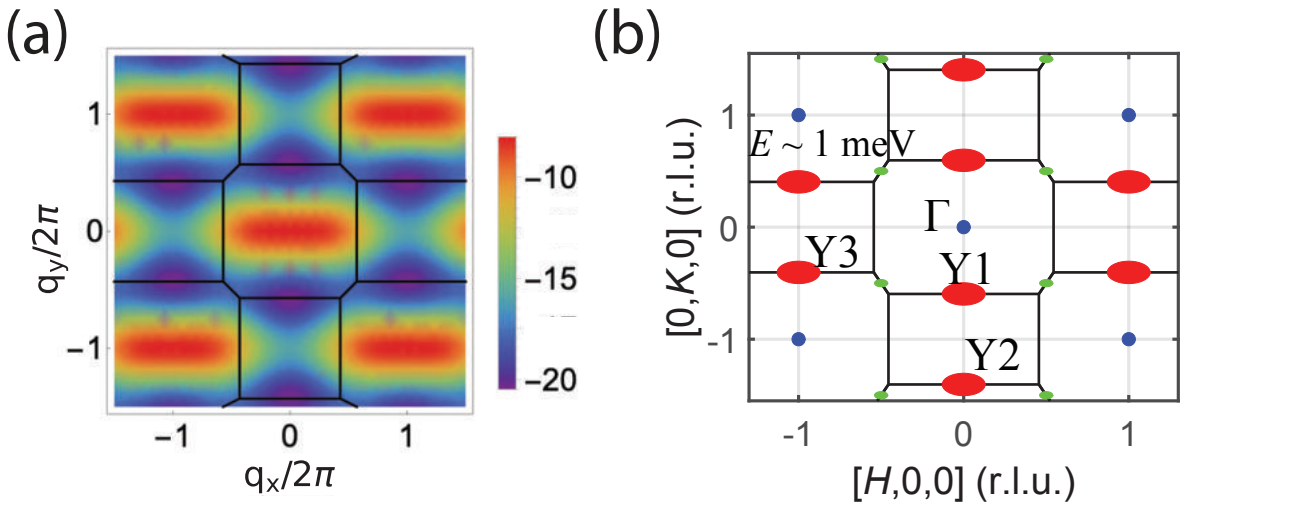


FIG. 5. (a) The exchange interaction eigenvalue, $J_{-}(\boldsymbol{q})$, plotted in the $(q_x, q_y)$ plane for $q_z = 0$ [Fig. 1(b) of the main text]. (b) The schematic plot of the INS pattern in the $[H, K, 0]$ plane that are marked as red ellipses [adapted from Ref. 30]. The minima of $J_{-}(\boldsymbol{q})$ in (a) are consistent with the spin excitation patterns observed in (b). In both (a) and (b), the Brillouin zone boundaries are marked by the solid black lines.

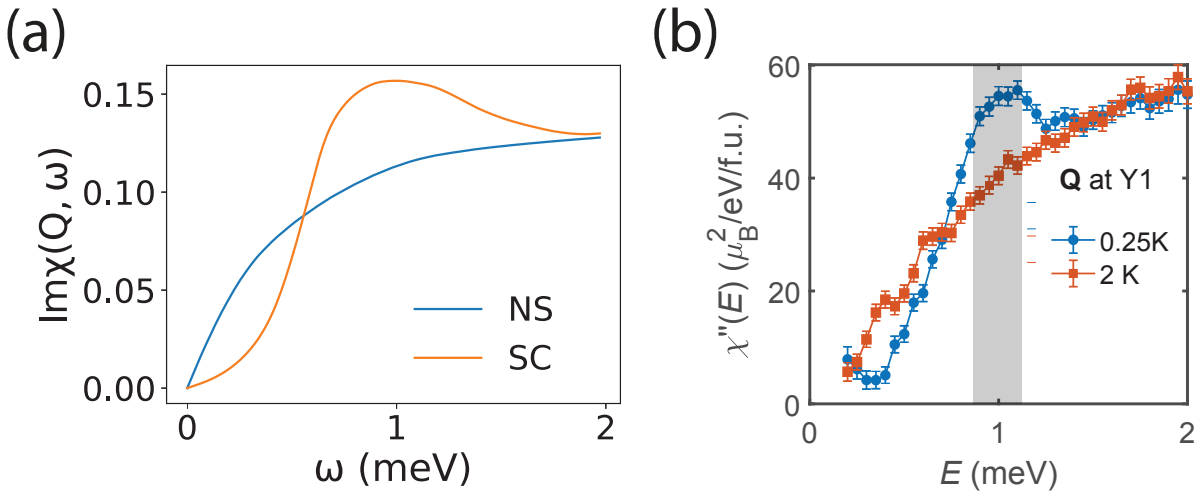


FIG. 6. (a) The imaginary part of the dynamical spin susceptibility as a function of energy in both the superconducting (SC) and normal (NS) states [ [Fig. 4(b) of the main text]. (b) The spin excitations observed at $K = 0.59, H = 0$ v.s. energy at $T = 0.25$ K (SC) and 2 K (NS) [adapted from Ref. 30]. The theoretical results capture the basic features of the experimental observations.

## PAIRING IN THE BAND BASIS

The kinetic term [Eq. 8] in the orbital basis $\Phi_{\boldsymbol{k}} = (A_\uparrow(\boldsymbol{k}), A_\downarrow(\boldsymbol{k}), B_\uparrow(\boldsymbol{k}), B_\uparrow(\boldsymbol{k}))$ [$j_\sigma = c_{j,\sigma}$, with $j = A, B$ for short-hand notation] can be diagonalized by a unitary matrix

$$U_{\boldsymbol{k}} = \frac{1}{\sqrt{2}} \begin{pmatrix} 0 & -u_{\boldsymbol{k}} & 0 & u_{\boldsymbol{k}} \\ -u_{\boldsymbol{k}} & 0 & u_{\boldsymbol{k}} & 0 \\ 0 & 1 & 0 & 1 \\ 1 & 0 & 1 & 0 \end{pmatrix}, \tag{15}$$

where $u_{\boldsymbol{k}} = \frac{\sqrt{\xi_x^2(\boldsymbol{k})+\xi_y^2(\boldsymbol{k})}}{\xi_x(\boldsymbol{k})+i\xi_y(\boldsymbol{k})}$.

The corresponding band dispersions are

$$\epsilon_\pm(\boldsymbol{k}) = \xi_0(\boldsymbol{k}) \pm \sqrt{\xi_x^2(\boldsymbol{k}) + \xi_y^2(\boldsymbol{k})}. \tag{16}$$

Each band is doubly degenerate due to the spin (of the Kramers doublet). We define the annihilation operators of lower and upper bands as $a$ and $b$, respectively, and let $\phi(\boldsymbol{k}) = (a_{k,\uparrow}, a_{k,\downarrow}, b_{k,\uparrow}, b_{k,\downarrow})^T$

The BdG Hamiltonian can be expressed in the Nambu basis $\psi(\boldsymbol{k}) = (a_{k,\sigma}, b_{k,\sigma}, \mathcal{T}a_{k,\sigma}^\dagger\mathcal{T}^{-1}, \mathcal{T}b_{k,\sigma}^\dagger\mathcal{T}^{-1})^T$, with $\mathcal{T}$ the time-reversal operator, as

$$H_{BdG}(\boldsymbol{k}) = \begin{pmatrix} E_k & \Delta_k \\ \Delta_k^* & -E_{-k} \end{pmatrix}, \tag{17}$$

where

$$\begin{aligned} E_k &= U_{\boldsymbol{k}}^\dagger H_{kin} U_{\boldsymbol{k}} = \begin{pmatrix} \epsilon_-(\boldsymbol{k}) & 0 \\ 0 & \epsilon_+(\boldsymbol{k}) \end{pmatrix} \otimes \sigma_0, \\ &= \begin{pmatrix} \xi_0(\boldsymbol{k}) - \sqrt{\xi_x^2(\boldsymbol{k}) + \xi_y^2(\boldsymbol{k})} & 0 \\ 0 & \xi_0(\boldsymbol{k}) + \sqrt{\xi_x^2(\boldsymbol{k}) + \xi_y^2(\boldsymbol{k})} \end{pmatrix} \otimes \sigma_0, \end{aligned} \tag{18}$$

and

$$\Delta_k = U_{\boldsymbol{k}}^\dagger \Delta_y U_{-\boldsymbol{k}} = \delta \begin{pmatrix} 0 & -id_1 & 0 & d_2 \\ id_1 & 0 & -d_2 & 0 \\ 0 & -d_2 & 0 & id_1 \\ d_2 & 0 & -id_1 & 0 \end{pmatrix}, \tag{19}$$

with $d_1 = \frac{\xi_y}{\sqrt{\xi_x^2+\xi_y^2}}$ and $d_2 = \frac{\xi_x}{\sqrt{\xi_x^2+\xi_y^2}}$. The intraband form factor $d_1$ is $p_z$-wave, and the interband form factor $d_2$ is $s$-wave. The dispersion of BdG Hamiltonian is

$$E_\pm(\boldsymbol{k}) = \sqrt{\delta^2 + \xi_0^2(\boldsymbol{k}) + \xi_x^2(\boldsymbol{k}) + \xi_y^2(\boldsymbol{k}) \pm 2\sqrt{\delta^2\xi_x^2(\boldsymbol{k}) + \xi_0^2(\boldsymbol{k})\xi_x^2(\boldsymbol{k}) + \xi_0^2(\boldsymbol{k})\xi_y^2(\boldsymbol{k})}} \tag{20}$$

where $E_-$ ($E_+$) corresponds to the band crossing (above) the Fermi energy. They can be further simplified as

$$\begin{aligned} E_\pm(\boldsymbol{k}) &= \sqrt{\delta^2 + \xi_0^2(\boldsymbol{k}) + \xi_x^2(\boldsymbol{k}) + \xi_y^2(\boldsymbol{k}) \pm 2\sqrt{\xi_x^2(\boldsymbol{k}) + \xi_y^2(\boldsymbol{k})}\sqrt{\xi_0^2(\boldsymbol{k}) + \delta^2\sin^2\phi(\boldsymbol{k})}} \\ &= \sqrt{\left(\sqrt{\xi_0^2(\boldsymbol{k}) + \delta^2\sin^2\phi(\boldsymbol{k})} \pm \sqrt{\xi_x^2(\boldsymbol{k}) + \xi_y^2(\boldsymbol{k})}\right)^2 + \delta^2(1 - \sin^2\phi(\boldsymbol{k}))} \end{aligned} \tag{21}$$

with $\sin\phi(\boldsymbol{k}) = \frac{\xi_x(\boldsymbol{k})}{\sqrt{\xi_x^2(\boldsymbol{k})+\xi_y^2(\boldsymbol{k})}}$. $E_-(\boldsymbol{k}) = 0$ requires both squared terms to be 0. The second term equals 0 in $k_z = 0, 2\pi$ planes where $\sin^2\phi_k = 1$. The first term goes to 0 when

$$\delta^2 = \xi_x^2(\boldsymbol{k}) + \xi_y^2(\boldsymbol{k}) - \xi_0^2(\boldsymbol{k}). \tag{22}$$

The Fermi surface is specified by $\xi_0 - \sqrt{\xi_x^2 + \xi_y^2} = 0$.

Finally, we show the explicit expressions that connect the fermion operators in the orbital and band bases:

$$\begin{aligned} A_\uparrow &= \frac{1}{\sqrt{2}}\left(-u_k a_\downarrow + u_k b_\downarrow\right) \\ A_\uparrow &= \frac{1}{\sqrt{2}}\left(-u_k a_\downarrow + u_k b_\downarrow\right) \\ B_\uparrow &= \frac{1}{\sqrt{2}}\left(a_\downarrow + b_\downarrow\right) \\ B_\downarrow &= \frac{1}{\sqrt{2}}\left(a_\downarrow + b_\downarrow\right) . \end{aligned} \tag{23}$$

## SELF-CONSISTENT DETERMINATION OF THE SPIN-TRIPLET PAIRING FUNCTION

We start from the anisotropic spin-exchange interactions (see main text), $I_x \gg I_z > I_y$, and thus consider

$$\begin{aligned} \hat{H}_{ex} =& \sum_i -I^x S^x_{i,A} S^x_{i,B} - I^y S^y_{i,A} S^y_{i,B} - I^z S^z_{i,A} S^z_{i,B} \\ =& \sum_i \frac{-I_x + I_y - I_z}{4}\frac{1}{4}\left(\Phi_i^\dagger [i\tau_y\sigma_0]\Phi_i^*\right)\left(\Phi_i^T[-i\tau_y\sigma_0]\Phi_i\right) \\ &+ \frac{I_x - I_y - I_z}{4}\frac{1}{4}\left(\Phi_i^\dagger [-\tau_y\sigma_z]\Phi_i^*\right)\left(\Phi_i^T[\tau_y\sigma_z]\Phi_i\right) \\ &+ \frac{-I_x - I_y + I_z}{4}\frac{1}{4}\left(\Phi_i^\dagger [\tau_y\sigma_x]\Phi_i^*\right)\left(\Phi_i^T[-\tau_y\sigma_x]\Phi_i\right) \\ &+ \frac{I_x + I_y + I_z}{4}\frac{1}{4}\left(\Phi_i^\dagger [i\tau_y\sigma_y]\Phi_i^*\right)\left(\Phi_i^T[-i\tau_y\sigma_y]\Phi_i\right) , \end{aligned} \tag{24}$$

where $\Phi_i = (A_\uparrow, A_\downarrow, B_\uparrow, B_\downarrow)_i^T$. The first three terms correspond to triplet pairing while the last term is the singlet pairing. The dominance of $I_x$ (together with $I_z > I_y$) implies that we can focus on the first term. We define

$$\delta_y = \langle B_\uparrow A_\uparrow + B_\downarrow A_\downarrow - A_\uparrow B_\uparrow - A_\downarrow B_\downarrow \rangle , \tag{25}$$

and perform Hubbard-Stratonovich transformation to Eq. 24. The effective Hamiltonian for our self-consistent analysis becomes

$$H_{eff} = \sum_{\boldsymbol{k}} \frac{1}{2}\begin{pmatrix} H_{kin}(\boldsymbol{k}) & -\Delta(\boldsymbol{k}) \\ -\Delta^\dagger(\boldsymbol{k}) & -H_{kin}(-\boldsymbol{k}) \end{pmatrix} - \frac{I_{eff}}{16}\delta_y^*\delta_y, \tag{26}$$

and the gap function $\Delta(\boldsymbol{k}) = \frac{I_{eff}\delta_y}{8} i\tau_y\sigma_0$, with $I_{eff} = I_x - I_y + I_z$. The pairing amplitude can now be determined self-consistently. We find $\delta = 0.6\mathrm{meV}$. The maximal value of the corresponding gap close to the Fermi surface is $\Delta = 0.44\mathrm{meV}$.

## SPIN RESONANCE IN A SINGLE-BAND SPIN-TRIPLET SUPERCONDUCTOR

For a single-band spin-triplet $\Delta_k\sigma^y$ pairing, the bare spin susceptibilities along three directions take the forms

$$\chi^{0,x}(\boldsymbol{q}, i\omega) = \frac{1}{4}\sum_k \frac{1}{2}\left(1 - \frac{\epsilon_k\epsilon_{k+q} - \Delta_k\Delta_{k+q}}{E_k E_{k+q}}\right)\left(\frac{1 - f(E_k) - f(E_{k+q})}{i\omega + E_k + E_{k+q}} + \frac{1 - f(E_k) - f(E_{k+q})}{-i\omega + E_k + E_{k+q}}\right) \tag{27}$$

$$\chi^{0,y}(\boldsymbol{q}, i\omega) = \frac{1}{4}\sum_k \frac{1}{2}\left(1 - \frac{\epsilon_k\epsilon_{k+q} + \Delta_k\Delta_{k+q}}{E_k E_{k+q}}\right)\left(\frac{1 - f(E_k) - f(E_{k+q})}{i\omega + E_k + E_{k+q}} + \frac{1 - f(E_k) - f(E_{k+q})}{-i\omega + E_k + E_{k+q}}\right) \tag{28}$$

$$\chi^{0,z}(\boldsymbol{q}, i\omega) = \frac{1}{4}\sum_k \frac{1}{2}\left(1 - \frac{\epsilon_k\epsilon_{k+q} - \Delta_k\Delta_{k+q}}{E_k E_{k+q}}\right)\left(\frac{1 - f(E_k) - f(E_{k+q})}{i\omega + E_k + E_{k+q}} + \frac{1 - f(E_k) - f(E_{k+q})}{-i\omega + E_k + E_{k+q}}\right) \tag{29}$$

where $\epsilon_k$ is the dispersion in the normal state, $\Delta_k$ is the gap function and $E_k = \sqrt{\epsilon_k^2 + \Delta_k^2}$ is the BdG spectrum. We notice that, the resonance depends on both the direction of the paring vector $\vec{d}$ and the symmetry of the form factor. If $\mathrm{sign}(\Delta_k) = \mathrm{sign}(\Delta_{k+q})$, the resonance appears in the plane perpendicular to the pairing direction. If $\mathrm{sign}(\Delta_k) = -\mathrm{sign}(\Delta_{k+q})$, the resonance appears in the susceptibility parallel to the pairing direction.

## NOTATION OF FOURIER TRANSFORM

We define primitive vectors of the primitive unit cell as

$$\boldsymbol{a}_1 = \frac{1}{2}(1,1,-1), \tag{30}$$
$$\boldsymbol{a}_2 = \frac{1}{2}(-1,1,1), \tag{31}$$
$$\boldsymbol{a}_3 = \frac{1}{2}(1,-1,1), \tag{32}$$

where there are two sublattices in the primitive unit cell. The corresponding reciprocal vectors are

$$\boldsymbol{b}_1 = 2\pi(0,1,1) \tag{33}$$
$$\boldsymbol{b}_2 = 2\pi(1,0,1) \tag{34}$$
$$\boldsymbol{b}_3 = 2\pi(1,1,0). \tag{35}$$

We then discuss the two different definitions of Fourier transformation:

$$c_{\boldsymbol{k},\alpha} = \sum_{\boldsymbol{R}} c_{i,\alpha} e^{-i\boldsymbol{k}\cdot\boldsymbol{R}_i},$$
$$\tilde{c}_{\boldsymbol{k},\alpha} = \sum_{\boldsymbol{R}} c_{i,\alpha} e^{-i\boldsymbol{k}\cdot(\boldsymbol{R}_i+\boldsymbol{r}_\alpha)},$$

where $\alpha$ is the sublattice index, $\boldsymbol{R}_i$ is the position of $i$-th primitive unit cell and $\boldsymbol{r}_\alpha$ is the position of sublattice $\alpha$ in each unit cell [$\boldsymbol{r_A} = (0,0,\eta/2), \boldsymbol{r_B} = (0,0,-\eta/2)$]. $\tilde{c}_{\boldsymbol{k},\alpha}$ explicitly includes the additional phase factor caused by the sublattice displacement and two definitions are connected by the following relation

$$c_{\boldsymbol{k},\alpha} = \tilde{c}_{\boldsymbol{k},\alpha} e^{i\boldsymbol{k}\cdot\boldsymbol{r_\alpha}}. \tag{36}$$

Correspondingly, we can define the Fourier transformation of spin operators as

$$S^\mu_\alpha(\boldsymbol{q}) = \sum_{\boldsymbol{R}} S^\mu_{i,\alpha} e^{-i\boldsymbol{q}\cdot\boldsymbol{R}_i} = \sum_{\boldsymbol{k}} c^\dagger_{\boldsymbol{k},\alpha}\sigma^\mu c_{\boldsymbol{k}+\boldsymbol{q},\alpha},$$
$$\tilde{S}^\mu_\alpha(\boldsymbol{q}) = \sum_{\boldsymbol{R}} S^\mu_{i,\alpha} e^{-i\boldsymbol{q}\cdot(\boldsymbol{R}_i+\boldsymbol{r}_\alpha)} = \sum_{\boldsymbol{k}} \tilde{c}^\dagger_{\boldsymbol{k},\alpha}\sigma^\mu \tilde{c}_{\boldsymbol{k}+\boldsymbol{q},\alpha},$$

where $\mu = x, y, z$. And

$$\boldsymbol{S}_\alpha(\boldsymbol{q}) = \tilde{\boldsymbol{S}}_\alpha(\boldsymbol{q}) e^{i\boldsymbol{q}\cdot\boldsymbol{r_\alpha}}. \tag{37}$$

The corresponding spin susceptibilities are

$$\chi^\mu_{\alpha\gamma}(\boldsymbol{q}, i\omega) = \langle S^\mu_\alpha(\boldsymbol{q}, i\omega) S^\mu_\gamma(-\boldsymbol{q}, -i\omega)\rangle$$
$$\tilde{\chi}^\mu_{\alpha\gamma}(\boldsymbol{q}, i\omega) = \langle \tilde{S}^\mu_\alpha(\boldsymbol{q}, i\omega) \tilde{S}^\mu_\gamma(-\boldsymbol{q}, -i\omega)\rangle,$$

which are related to each other via

$$\chi^\mu_{\alpha\gamma}(\boldsymbol{q}, i\omega) = \tilde{\chi}^\mu_{\alpha\gamma}(\boldsymbol{q}, i\omega) e^{i\boldsymbol{q}\cdot(\boldsymbol{r}_\alpha - \boldsymbol{r}_\gamma)}. \tag{38}$$

In the main text, we use the definition of $c_{\boldsymbol{k},\alpha}$ and $\boldsymbol{S}_\alpha(\boldsymbol{q})$ in order to simplify the notation. However, in the calculation of dynamical spin susceptibility, we transform back to the $\tilde{\chi}$ via Eq. 38 and sum over all the scattering channels. The final spin susceptibilities are defined as

$$\begin{aligned}\chi^\mu(\boldsymbol{q}, i\omega) &= \sum_{\alpha\gamma} \tilde{\chi}^\mu_{\alpha\gamma}(\boldsymbol{q}, i\omega) = \sum_{\alpha\gamma} \chi^\mu_{\alpha\gamma}(\boldsymbol{q}, i\omega) e^{-i\boldsymbol{q}\cdot(\boldsymbol{r_\alpha} - \boldsymbol{r_\gamma})} \\ &= \chi^\mu_{AA}(\boldsymbol{q}, i\omega) + \chi^\mu_{BB}(\boldsymbol{q}, i\omega) + \chi^\mu_{AB}(\boldsymbol{q}, i\omega) e^{-i\boldsymbol{q}\cdot(\boldsymbol{r}_A - \boldsymbol{r}_B)} + \chi^\mu_{BA}(\boldsymbol{q}, i\omega) e^{-i\boldsymbol{q}\cdot(-\boldsymbol{r}_A + \boldsymbol{r}_B)}.\end{aligned} \tag{39}$$

We note that for $q_z = 0$, in Fig. 4, $\tilde{\chi} = \chi$.

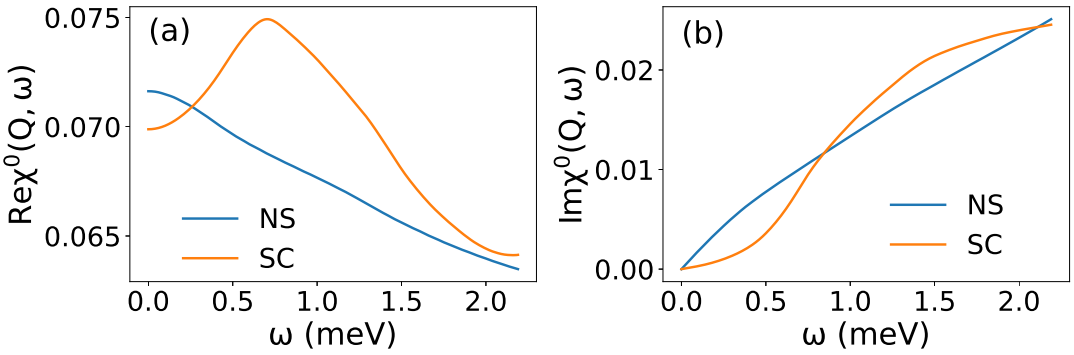


FIG. 7. (a) The real part and (b) the imaginary part of the bare spin susceptibility in the normal state (NS) and superconducting state (SC).

## CALCULATION OF SPIN RESONANCE

We utilize the random phase approximation (RPA) to calculate the dynamical spin susceptibility of the spin-$x$ component in the spin-triplet $\Delta_y$ pairing case. The corresponding equations in matrix form are

$$\chi(\boldsymbol{q}, i\omega) = \chi^0(\boldsymbol{q}, i\omega)[\mathbb{I} + J(\boldsymbol{q})\chi^0(\boldsymbol{q}, i\omega)]^{-1}, \tag{40}$$

where $\chi^0$ is the bare susceptibility with the following matrix:

$$\chi^0(\boldsymbol{q}, i\omega) = \begin{pmatrix} \chi^0_{AA}(\boldsymbol{q}, i\omega) & \chi^0_{AB}(\boldsymbol{q}, i\omega) \\ \chi^0_{BA}(\boldsymbol{q}, i\omega) & \chi^0_{BB}(\boldsymbol{q}, i\omega) \end{pmatrix}. \tag{41}$$

In practice, the dominant contributions to the low frequency spin susceptibility come from the intraband processes of the lowest band. Using Eq. 23, we approximately calculate bare spin susceptibility via

$$\chi^0(\boldsymbol{q}, i\omega) = \sum_{\boldsymbol{k}} \begin{pmatrix} \chi^0_{aa}(\boldsymbol{q}, \boldsymbol{k}, i\omega) & u^*_{\boldsymbol{k}+\boldsymbol{q}} u_{\boldsymbol{k}} \chi^0_{aa}(\boldsymbol{q}, \boldsymbol{k}, i\omega) \\ u_{\boldsymbol{k}+\boldsymbol{q}} u^*_{\boldsymbol{k}} \chi^0_{aa}(\boldsymbol{q}, \boldsymbol{k}, i\omega) & \chi^0_{aa}(\boldsymbol{q}, \boldsymbol{k}, i\omega) \end{pmatrix}, \tag{42}$$

where $\chi^0_{aa}$ denotes the contribution from the lowest bands and

$$\chi^0_{aa}(\boldsymbol{q}, \boldsymbol{k}, i\omega) \sim \sum_k \frac{1}{2}\left(1 - \frac{\epsilon_-(\boldsymbol{k})\epsilon_-(\boldsymbol{k}+\boldsymbol{q}) - d_1(\boldsymbol{k})d_1(\boldsymbol{k}+\boldsymbol{q})}{E_-(\boldsymbol{k})E_-(\boldsymbol{k}+\boldsymbol{q})}\right) \frac{1 - f(E_-(\boldsymbol{k})) - f(E_-(\boldsymbol{k}+\boldsymbol{q}))}{-i\omega + E_-(\boldsymbol{k}) + E_-(\boldsymbol{k}+\boldsymbol{q})}. \tag{43}$$

From the above equations, we can calculate $\chi_{\alpha\gamma}(\boldsymbol{q}, i\omega)$. In turn, the total spin susceptibility is given by $\chi(\boldsymbol{q}, i\omega) = \sum_{\alpha\gamma} \chi_{\alpha\gamma}(\boldsymbol{q}, i\omega) e^{-i\boldsymbol{q}\cdot(\boldsymbol{r}_\alpha - \boldsymbol{r}_\gamma)}$.

## BARE SUSCEPTIBILITIES

Here, we present the bare susceptibility along $x$ direction

$$\chi^0(Q, i\omega) = \sum_{\alpha,\gamma} \chi^0_{\alpha\gamma}(Q, i\omega) e^{-iQ\cdot(\boldsymbol{r}_\alpha - \boldsymbol{r}_\gamma)} \tag{44}$$

of both the normal state (NS) and the superconducting state (SC) in Fig. 7.

## MAGNETIC EXCHANGE INTERACTIONS INFERRED FROM INS EXPERIMENTS

As an application of Eq. 39, we consider the classical limit and suppose the magnetic form factor of individual $U$ atoms as $f_\alpha(\boldsymbol{q})$ ($\alpha = A/B$) and suppose the coherent factor $u_k = 1$ everywhere, which means $\chi_{AA}(\boldsymbol{q}) = \chi_{BB}(\boldsymbol{q}) = f^2(\boldsymbol{q})$ and $\chi_{AB}(\boldsymbol{q}) = \chi_{BA}(\boldsymbol{q}) = f_A(\boldsymbol{q}) f_B(\boldsymbol{q})$. Eq. 39 can be reorganized as

$$\chi^\mu(\boldsymbol{q}) = 2f^2(\boldsymbol{q}) + f_A(\boldsymbol{q}) f_B(\boldsymbol{q}) e^{i\boldsymbol{q}(\boldsymbol{r}_A - \boldsymbol{r}_B)} + f_A(\boldsymbol{q}) f_B(\boldsymbol{q}) e^{-i\boldsymbol{q}(\boldsymbol{r}_A - \boldsymbol{r}_B)}. \tag{45}$$

If the magnetic correlation between $A$ and $B$ sublattices within the same unit cell is ferromagnetic, i.e. $f_A(\boldsymbol{q}) = f_B(\boldsymbol{q}) = f(\boldsymbol{q})$, then $\chi^{\mu}_{AB} = \chi^{\mu}_{AB} > 0$ and we have

$$\begin{aligned}\chi^{\mu}(\boldsymbol{q}) &= f^2(\boldsymbol{q})\,(2 + 2\cos q_z\eta) \\ &= 4f^2(\boldsymbol{q})\cos^2\frac{q_z\eta}{2}.\end{aligned} \tag{46}$$

For the antiferromagnetic correlation($f_A(\boldsymbol{q}) = -f_B(\boldsymbol{q}) = f(\boldsymbol{q})$), $\chi^{\mu}_{AB} = \chi^{\mu}_{AB} < 0$, and we have

$$\begin{aligned}\chi^{\mu}(\boldsymbol{q}) &= f^2(\boldsymbol{q})\,(2 - 2\cos q_z\eta) \\ &= 4f^2(\boldsymbol{q})\sin^2\frac{q_z\eta}{2}.\end{aligned} \tag{47}$$

Following Eqs. 46, 47, the inelastic neutron-scattering results imply that the correlation between $A$ and $B$ sublattices are FM, thereby suggesting a ferromagnetic $I$ [28].

Further experimental constraints, on $J_{r\geq 2}$, are less direct, and are primarily based on the wavevector for the observed AF correlations. The observed $Q_y \gtrsim \pi$ suggests that both $J_4$ and $J_2$ are AF. Likewhise, the observed $Q_x = 0$ suggests that $J_3$ is FM.